OBSERVATION OF EVENTS AT VERY HIGH Q^2 in ep COLLISIONS AT HERA

E. Elsen
DESY, Notkestr. 85,
22607 Hamburg, Germany

H1 Collaboration

Deep-inelastic ep scattering has been studied up to the largest momentum transfers Q^2 presently accessible at HERA. For $Q^2 > 15000\,\mathrm{GeV}^2$, 12 neutral current candidate events are observed where the expectation from the Standard Model of deep-inelastic scattering is 4.71 ± 0.76 events. In the same kinematical range 4 candidate events for the charged current process are observed while 1.77 ± 0.87 events are expected. The difference between observed and expected number of events for the neutral current process seems to be pronounced when the positron is backscattered at large angles.

1 Introduction

HERA, the first ep collider ever, allows to probe the proton at distances down to $\simeq 10^{-16}\,\mathrm{cm}$ via t-channel exchange of a highly virtual gauge boson [1,2,3], and to search in the s-channel for new particles that couple to lepton-parton pairs with masses up to the kinematic limit of $\sqrt{s} \simeq 300\,\mathrm{GeV}$ [4].

We report on a measurement of neutral and charged current deep-inelastic scattering using all e^+p data recorded with the H1 detector at HERA from 1994 to 1996. The data refer to an integrated luminosity of $14.19 \pm 0.32\,\mathrm{pb}^{-1}$ at beam energies of 27.5 GeV and 820 GeV for the positrons and protons, respectively.

A full account of the analysis has been given in a more detailed report [5]. This reference together with the observation of the ZEUS collaboration [6] should be consulted for further details. Here we confine ourselves to a description of the main observations.

2 The H1 Detector

The essential components of the H1 detector [7] for this analysis are the calorimeter and the tracking system.

The positron[a] energy and angle are measured in a liquid argon (LAr) calorimeter covering the polar angular range $4^\circ \leq \theta \leq 153^\circ$ and all azimuthal angles. The granularity is optimized to provide approximately uniform segmentation in laboratory pseudorapidity and azimuthal angle ϕ. The lead/argon

[a] We do not explicitly distinguish electrons and positrons in this analysis.

electromagnetic section is followed by a stainless steel/argon hadronic section. Energies of electromagnetic showers can be reconstructed with a precision of $\sigma(E)/E \sim 12\%\sqrt{E/\mathrm{GeV}} \oplus 1\%$ and pion induced hadronic energies with a resolution $\sigma(E)/E \sim 50\%/\sqrt{E/\mathrm{GeV}} \oplus 2\%$ after software energy weighting. The absolute energies are known to 3% and 4% for electromagnetic and hadronic energies, respectively.

Located inside the calorimeter is the tracking system which is exploited to determine the interaction vertex. It consists of central drift and proportional chambers ($25^\circ \leq \theta \leq 155^\circ$), a forward track detector ($7^\circ \leq \theta \leq 25^\circ$). Both calorimeters and tracking system are surrounded by a 1.15 T superconducting field parallel to the z axis[b]. The iron return yoke is instrumented to measure leakage of hadronic showers and to register muons.

The luminosity is measured from the rate of the Bethe-Heitler $ep \to ep\gamma$ bremsstrahlung, when the e and γ are tagged in coincidence 33 and 103 m behind the experiment.

3 Event Selection and Kinematics

The initial selection yields a proper sample of ep interactions by exploiting topology and time of arrival such that the resulting event sample can be considered free of background from beam gas, cosmic rays and beam halo events. The deep-inelastic final state is separated from competing background processes by selecting events based on the topology of signals in the detector and reconstructed kinematics.

3.1 Kinematics

The kinematics of lepton-proton scattering at fixed collider beam energies is described by two independent variables. Several Lorentz invariant quantities can be calculated of which the most common are

$$Q^2 = -q^2 = (k - k')^2 \tag{1}$$

$$y = \frac{Pq}{Pk} = \frac{1}{2}(1 + \cos\theta^*) \tag{2}$$

$$x = \frac{Q^2}{2Pq} \tag{3}$$

[b] The z axis is taken to follow the direction of the incident proton beam.

$$M = \sqrt{sx} \tag{4}$$

where k and P refer to the 4-vectors of the incoming e and p beams and k' to the 4-vector of the scattered positron. Q^2 describes the virtuality of the exchanged boson, while in the parton picture y and M refer to the scattering angle θ^* in the CM system and the mass, respectively, of the e-quark interaction.

Experimentally, convenient approximations are based on using

$$Q^2 = \frac{P_T^2}{(1-y)} \tag{5}$$

where transverse momentum P_T is measured from either the scattered lepton, the transverse momentum of the scattered jet or both. The different methods are described in detail in the appendix.

3.2 Neutral Current Selection

NC DIS events in the high Q^2 domain are selected by imposing the following cuts which are based on measurements of the calorimeter energy deposits and a detailed study of the transverse and longitudinal shower profiles:

- an isolated positron with $E_{T,e} > 25\,\mathrm{GeV}$ found within the polar angle $10^o < \theta < 145^o$,
- a total transverse momentum balance $P_{T,miss}/\sqrt{E_{T,miss}} < 3\sqrt{\mathrm{GeV}}$,
- a limited momentum loss in the direction of the incident positron, $43 < \sum(E - p_z) < 63\,\mathrm{GeV}$.

The second cut takes into account the natural scale of the energy for determination of the hadronic energy resolution. The last cut exploits the fact that the $\sum(E - p_z)$ distribution is peaked at $2E_e$ and provides a safeguard against catastrophic initial state radiation where the collinear γ is not reconstructed in the detector.

In addition the analysis is restricted to the kinematic range $Q^2 > 2500\,\mathrm{GeV}^2$ and $0.1 < y < 0.9$ for which 471 NC DIS events are retained.

3.3 Charged Current Selection

CC DIS events are selected by imposing the following cut:

- a total missing transverse momentum $P_{T,miss} > 50\,\mathrm{GeV}$,

- a total transverse energy to match $P_{T,miss}$ such that $P_{T,miss}/E_T > 0.5$.

In addition the analysis is restricted to the kinematic range $Q^2 > 2500\,\mathrm{GeV}^2$ and $y < 0.9$, for which 31 CC DIS events are retained.

4 Standard Model of Deep-Inelastic Scattering

The expectation for NC and CC DIS ep scattering is based on the parton model in the approximation of single γ/Z and W exchange. Detailed expressions for the cross-sections, which contain a description of the proton in terms of scale dependent structure functions, can be found in reference [3]. The structure functions themselves are expressed in terms of parton densities obtained from global fits to fixed target data[8], inclusive lepton and photon production data[9] and to low Q^2 measurements at HERA [10].

For the purpose of comparison to data a Monte Carlo simulation using the event generator DJANGO [11] is performed followed by a full simulation of the response of the H1 detector.

The residual systematic uncertainties are subdivided into *experimental* uncertainties of $\pm 2.3\%$ on the integrated luminosity, $\pm 3\%$ on the absolute energy scale of the electromagnetic calorimeter and $\pm 4\%$ on the absolute energy scale of the calorimeter response to hadronic showers and *theoretical* uncertainties. The latter encompass $\pm 5\%$ on the uncertainty of parton density distributions, $\pm 4\%$ on the value of the strong coupling constant α_s and $\pm 2\%$ from the uncertainty of QED corrections in the y range considered for this analysis.

5 Backgrounds

Contributions from background processes giving rise to true or misidentified isolated positrons at high E_T or events with a large $P_{T,miss}$ were evaluated using the full simulation program. The background processes considered comprise production of real vector bosons Z and W, photoproduction at large E_T and $\gamma\gamma$ processes. After introducing specific additional requirements in the selection of the events with only minor effect on the DIS sample the sum of these processes is seen to contribute [5] less than 0.1 events at large Q^2. The purity of these selections was verified by relaxing the quality criteria for the scattered positron and by visual inspection of the events.

6 Analysis

We find 443 events in the NC DIS sample for an expectation of 427 ± 38 events. The 31 observed CC events are in good agreement with 34.2 ± 5.8 from CC

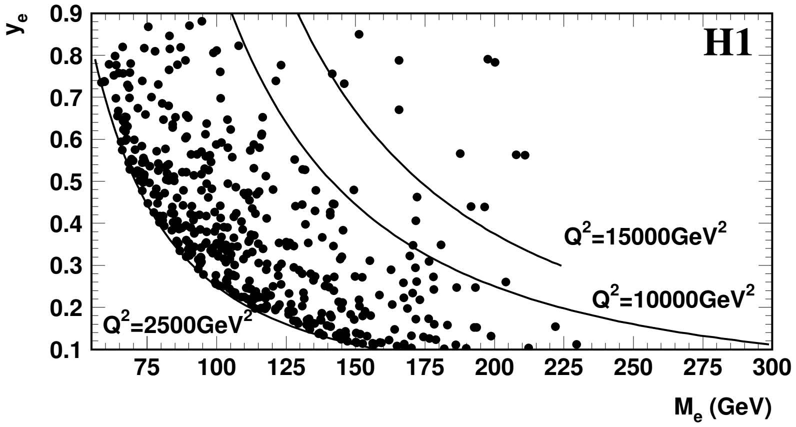

Figure 1: Selected NC DIS candidates in the M_e-y_e plane. Contours of fixed Q^2 are also indicated

DIS processes. Due to the inherent kinematical redundancy the selected NC events themselves can be used to study the resolutions of the reconstructed quantities. We take the e-method, which provides the best resolution at large y, as a reference. We find good agreement for the mass reconstruction using the other methods; in particular even the h-method, which is the only method for reconstruction in CC events, is seen to give good agreement, albeit at significant lower resolution $\approx 10\,\mathrm{GeV}$. The distributions are well reproduced by Monte Carlo simulations. It should be noted that also the direct reconstruction of the invariant mass $M_{e+\mathrm{jet}}$ is well reproduced, reminiscent of the fact that the measurement is dominated by hard $e + \mathrm{parton} \to e + \mathrm{parton}$ scattering leading to a final state with one single hadronic jet.

Fig. 1 shows the two dimensional distribution of y_e against M_e, which is cut-off at low y_e and M_e due to the requirement $Q^2 > 2500\,\mathrm{GeV}^2$. Specific projections are shown in fig. 2 together with the expectations from the standard DIS model. It can be seen that for lower Q^2 the simulation well reproduces the observed distributions while at large masses M_e an excess seems to appear in the data, which is more pronounced for large y_e.

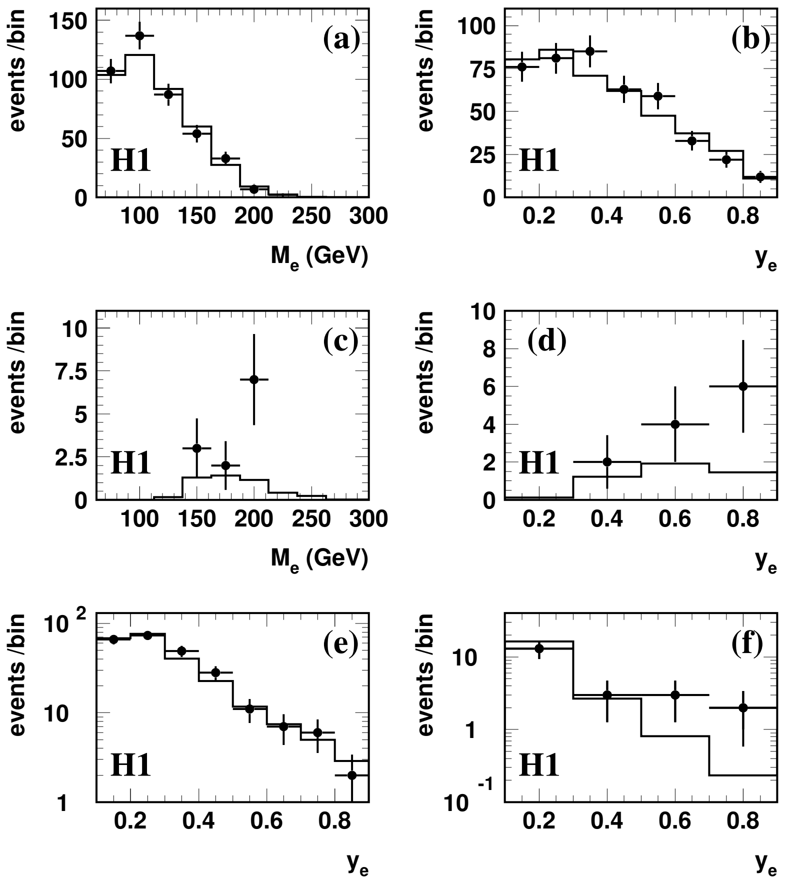

Figure 2: Distributions of M_e and y_e for selected NC DIS candidate events, (a) and (b) for $2500 < Q^2 < 15000\,\mathrm{GeV}^2$, (c) and (d) for $Q^2 > 15000\,\mathrm{GeV}^2$; distribution of y_e (e) for $100 < M_e < 180\,\mathrm{GeV}$ and (f) for $M_e > 180\,\mathrm{GeV}$ together with the expectation from NC DIS.

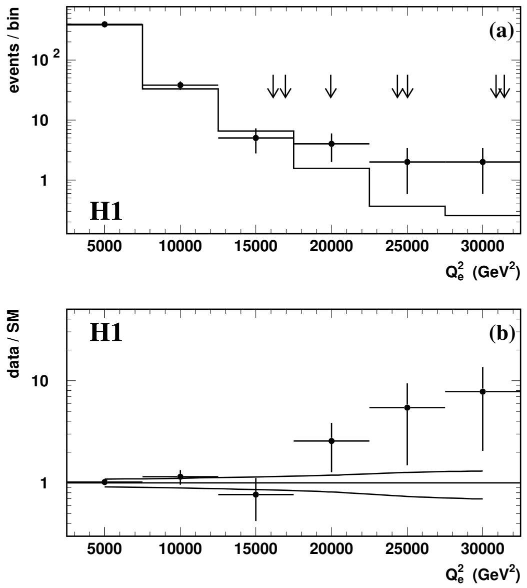

Figure 3: (a) Q^2-distribution of the selected NC DIS candidate events for $Q^2 > 15000\,\mathrm{GeV}^2$ and $M_e > 180\,\mathrm{GeV}$ together with the expectation from NC DIS; (b) the ratio of the two distribution together with the 1σ error contours.

6.1 Q^2 Dependence

In order to assess the uncertainties in the expected Q^2 distribution fig. 3 shows the comparison of the NC data with the simulation. The uncertainties are small compared to the deviations of the data points from expectation at large Q^2, albeit with large statistical uncertainty. For $Q^2 > 15000\,\mathrm{GeV}^2$, 12 events are observed while 4.71 ± 0.76 events are expected. The associated Poisson probabilities including the systematic uncertainty of the expectation assume values of 1% at the largest values of Q^2 values.

The statistical uncertainty for the CC DIS data is considerably larger. With 4 events observed for an expectation of 1.77 ± 0.87 events for $Q^2 > 15000\,\mathrm{GeV}^2$ not much can be concluded.

6.2 Events at Very High Q^2, M and y

The mass distributions of the NC data for two lower cutoffs of y are shown in fig. 4 together with the expectation. The expectation well reproduces the data up to masses of $\approx 150\,\mathrm{GeV}$ when the data start to consistently overshoot the expectation. At $M_e \approx 200\,\mathrm{GeV}$ the data are several standard deviations above the expectation; the difference is most pronounced at large y_e.

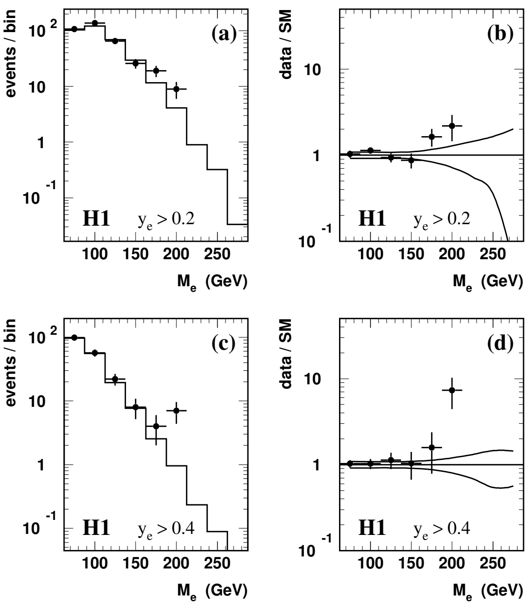

Figure 4: (a) Distribution of M_e for the observed NC DIS candidates with $y_e > 0.2$. The expectation from standard NC DIS is shown as a superimposed histogram; (b) ratio of the observed and expected number of events as a function of M_e for $y_e > 0.2$; the lines above and below "1" specify the $\pm 1\sigma$ levels of uncertainty for the standard NC DIS expectation; (c) as in (a) and (d) as in (b) but now with $y_e > 0.4$.

In order to quantify this difference we use Poisson probabilities to calculate the probabilities for the observation. We find a value of 2.6×10^{-4} for the data to fluctuate to the number of events observed in the interval $M_e = 200 \pm 12.5\,\mathrm{GeV}$. This probability does not reflect the fact that such a fluctuation may occur *anywhere* in the kinematical plane. If we take such variations into

Table 1: The results of various methods of determining the kinematics of the seven events satisfying the cuts $M_e > 180\,\mathrm{GeV}$ and $y > 0.4$

M [GeV]				y			Q^2 [$10^3\,\mathrm{GeV}^2$]		
e	2α	Σ	$e-\mathrm{j}$	e	2α	Σ	e	2α	Σ
196(5)	198	196	195	.439(14)	.434	.443	17.0(4)	17.1	17.1
208(4)	200	209	213	.563(12)	.582	.592	24.4(4	23.3	25.9
188(12)	185	188	184	.566(32)	.573	.561	20.0(14)	19.6	19.8
198(2)	199	196	197	.790(8)	.787	.786	30.9(5)	31.3	30.2
211(4)	227	210	211	.562(12)	.526	.525	25.0(4)	27.1	23.1
192(6)	190	190	215	.440(16)	.443	.501	16.1(4)	16.1	18.1
200(2)	213	202	210	.783(8)	.762	.786	31.4(5)	34.5	31.9

account we find a probability of less than 1% to obtain a minimum as small as we observe around 200 GeV.

The seven events of fig. 1 satisfying $M_e > 180\,\mathrm{GeV}$ and $y > 0.4$ have been studied in more detail. Their kinematic reconstruction is given in table 1. Beautiful agreement is seen for all reconstruction methods, both evidence for the reliable reconstruction of the kinematics of these events and a sign of lack of catastrophic initial state bremsstrahlung.

7 Non-Standard Contributions at high Q^2

7.1 New Contributions in the Standard DIS Model

We have tried to assess the uncertainties in the expectation of the standard DIS model by (a) varying the parton distribution functions, (b) assuming different values for the strong coupling constant α_s, (c) modifying the hadronisation scheme and (d) allowing F_L, the longitudinal structure function, to be non zero. We do observe considerable reductions of the cross section, but no enhancement exceeding 20% of the standard value - hence falling short of explaining the effect. Within the standard DIS model the only explanation is therefore a statistical fluctuation.

7.2 Beyond the Standard DIS Model

Beyond the standard model new particles could be produced in the positron-parton system. Examples of these are leptoquarks, leptogluons and squarks in R-parity violating versions of Supersymmetry. They would show up as narrow resonances in the M distribution, although QED and QCD corrections would lead to significant broadening. At the present level of statistics no firm conclusion can be drawn from the observation. In contrast to the above, the virtual exchange of new particles between positrons and partons or possible substructure of fermions inducing contact interactions could lead to a mere enhancement of the cross-section at high Q^2.

8 Summary

The observed excess of data above standard model DIS expectations at large Q^2 or conversely at large x and y is intriguing since it appears in a corner of phase space where new effects are not yet (fully) excluded by other experiments. It also happens to be in a region where data is still scarce and hence implies a concentrated effort to collect more data at the highest Q^2. The running period of 97 is well under way and all effort will be made to maximize the luminosity yield to exclude the statistical uncertainties that presently are related with this measurement.

Acknowledgments

I wish to thank the organisers of the 1997 Lake Louise Winter Institute for providing a very stimulating atmosphere for physics discussions in the beautiful surroundings of the Rocky Mountains. In particular, I wish to thank F. Khanna and B. Campbell for the extra support in traveling on very short notice.

Appendix

The properties of the different reconstruction methods are quickly summarized below. A more detailed account can be found elsewhere [12]:

e-method uses the angle and energy of the scattered positron. It provides the best resolution for H1. The resolution in M deteriorates $\propto \frac{1}{y}$ and is shifted towards smaller values with large initial state radiation.

2α-method uses only the angles of the scattered positron and of the scattered jet $\tan(\theta_h/2) = \frac{\sum(E-p_z)}{(\sum p_{x,h}^2+\sum p_{y,h}^2)^{1/2}}$. Value is shifted upwards by initial state radiation.

Table 2: Formulae for determining the kinematics of the final states from the scattered positron e or the observed hadrons h

Reconstruction Method	Kinematic Quantity y	Q^2
e	$1 - \frac{E'_e}{E_e} \sin^2 \frac{\theta_e}{2}$	$4E_eE'_e \cos^2 \frac{\theta_e}{2}$
2α	$\tan \frac{\theta_h}{2} (\tan \frac{\theta_h}{2} + \tan \frac{\theta_e}{2})^{-1}$	$4E_e^2 (\tan \frac{\theta_e}{2} (\tan \frac{\theta_e}{2} + \tan \frac{\theta_h}{2}))^{-1}$
h	$\frac{\sum (E - p_z)}{2E_e}$	$\frac{\sum p_{x,h}^2 + \sum p_{y,h}^2}{1 - y_h}$
Σ	$\frac{\sum (E - p_z)}{\sum (E - p_z) + (E'_e - p_{z,e})}$	${E_e}^2 \sin^2 \theta_e / (1 - y_\Sigma)$

Σ-method Properties similar to the 2α method. However, to first order there is no effect of initial state radiation since the energy of the scattered electron is explicitly taken into account.

h-method uses angles and energies of the reconstructed hadrons. While the resolution is considerably reduced it is the only method available for *charged current* event reconstruction.

References

1. ZEUS Collaboration, M. Derrick et al., *Z. Phys.* C **67**, 81 (1995); H1 Collaboration, S. Aid et al., *Phys. Lett.* B **353**, 578 (1995);ZEUS Collaboration, M. Derrick et al., *Z. Phys.* C **72**, 47 (1996).
2. H1 Collaboration, S. Aid et al., *Z. Phys.* C **67**, 565 (1995).
3. H1 Collaboration, S. Aid et al., *Phys. Lett.* B **379**, 319 (1996).
4. H1 Collaboration, I. Abt et al., *Nucl. Phys.* B **396**, 3 (1993); ZEUS Collaboration, M. Derrick et al., *Phys. Lett.* B **306**, 173 (1993); H1 Collaboration, T. Ahmed et al., *Z. Phys.* C **64**, 545 (1994); H1 Collaboration, S. Aid et al., *Phys. Lett.* B **369**, 173 (1996); H1 Collaboration, I.

Abt et al., *Z. Phys.* C **71**, 211 (1996); ZEUS Collaboration, M. Derrick et al., *Z. Phys.* C **73**, 613 (1997).

5. H1 Collaboration, C. Adloff, et al., *Z. Phys.* C **74**, 191 (1997).
6. ZEUS Collaboration, J. Breitweg, et al., *Z. Phys.* C **74**, 207 (1997).
7. H1 Collaboration, I. Abt et al., *Nucl. Instrum. Methods* A **386**, 310 (1997); H1 Collaboration, I. Abt et al., *Nucl. Instrum. Methods* A **386**, 348 (1997)
8. BCDMS Collaboration, A.C. Benvenuti et al., *Phys. Lett.* B **223**, 485 (1989); CERN preprint CERN-EP/89-06 NMC Collaboration, P. Amaudruz et al., *Phys. Lett.* B **295**, 159 (1992); CCFR Collaboration, A.O. Bazarko et al., Proc. of the XXVIIIthe Renc. de Moriond, J. Trân Thanh Vân (Editor), March 1993 4pp.; EMC Collaboration, J.J. Aubert et al., *Nucl. Phys.* B **213**, 31 (1982)
9. WA70 Collaboration, M. Bonesini et al., *Z. Phys.* C **38**, 371 (1988); E605 Collaboration, C.N. Brown et al., *Phys. Rev. Lett.* **63**, 2637 (1989); CDF Collaboration, F. Abe et al., *Phys. Rev. Lett.* **68**, 2734 (1992); *idem Phys. Rev.* D **48**, 2998 (1993); *Phys. Rev. Lett.* **69**, 28 (1992); *idem Phys. Rev.* D **50**, 5550 (1994); *Phys. Rev.* D **50**, 2966 (1994); A. Bodek, CDF Collaboration, Proc. of the International Workshop on Deep-Inelastic Scattering, Eilat, Israel (1994); UA6 Collaboration, G. Sozzi et al., *Phys. Lett.* B **317**, 243 (1993).
10. H1 Collaboration, I. Abt et al., *Nucl. Phys.* B **407**, 515 (1993); ZEUS Collaboration, M. Derrick et al., *Phys. Lett.* B **316**, 412 (1993).
11. DJANGO 6.2, G.A. Schuler and H. Spiesberger, Proc. of the Workshop "Physics at HERA", W. Buchmüller and G. Ingelman (Editors), Oct. 1991, DESY Hamburg, Vol. 3, p. 1419;
12. S. Bentvelsen, J. Engelen and P. Kooijman, Proc. of the Workshop "Physics at HERA", W. Buchmüller and G. Ingelman (Editors), Oct. 1991, DESY Hamburg, Vol. 1, p. 25; K.C. Hoeger, *ibid*, p. 43.